BABAR-CONF-02/09
SLAC-PUB-9232

Measurements of the branching fractions of charmless three-body charged B decays

The *BABAR* Collaboration

May 31, 2002

Abstract

We present preliminary results of searches for charged B mesons decaying into the charmless three-body final states $h^{\pm}h^{\mp}h^{\pm}$, where $h = \pi$ or K, using 51.5 fb^{-1} of data collected at the $\Upsilon(4S)$ resonance with the *BABAR* detector at the SLAC PEP-II asymmetric B Factory. No assumptions are made about intermediate resonances. We measure the branching fractions $\mathcal{B}(B^{\pm} \to K^{\pm}\pi^{\mp}\pi^{\pm}) = (59.2 \pm 4.7 \pm 4.9) \times 10^{-6}$ and $\mathcal{B}(B^{\pm} \to K^{\pm}K^{\mp}K^{\pm}) = (34.7 \pm 2.0 \pm 1.8) \times 10^{-6}$, where the first error is statistical and the second error is systematic. In the same study, we do not observe significant signals for the final states $B^{\pm} \to \pi^{\pm}\pi^{\mp}\pi^{\pm}$ and $B^{\pm} \to K^{\pm}K^{\mp}\pi^{\pm}$, and therefore provide the 90% confidence upper limits $\mathcal{B}(B^{\pm} \to \pi^{\pm}\pi^{\mp}\pi^{\pm}) < 15 \times 10^{-6}$ and $\mathcal{B}(B^{\pm} \to K^{\pm}K^{\mp}\pi^{\pm}) < 7 \times 10^{-6}$.

Presented at the Flavor Physics and CP Violation (FPCP) Conference,
5/16 – 5/18/2002, Philadelphia, USA

Stanford Linear Accelerator Center, Stanford University, Stanford, CA 94309

Work supported in part by Department of Energy contract DE-AC03-76SF00515.

The *BABAR* Collaboration,

B. Aubert, D. Boutigny, J.-M. Gaillard, A. Hicheur, Y. Karyotakis, J. P. Lees, P. Robbe, V. Tisserand, A. Zghiche

Laboratoire de Physique des Particules, F-74941 Annecy-le-Vieux, France

A. Palano, A. Pompili

Università di Bari, Dipartimento di Fisica and INFN, I-70126 Bari, Italy

G. P. Chen, J. C. Chen, N. D. Qi, G. Rong, P. Wang, Y. S. Zhu

Institute of High Energy Physics, Beijing 100039, China

G. Eigen, I. Ofte, B. Stugu

University of Bergen, Inst. of Physics, N-5007 Bergen, Norway

G. S. Abrams, A. W. Borgland, A. B. Breon, D. N. Brown, J. Button-Shafer, R. N. Cahn, E. Charles, M. S. Gill, A. V. Gritsan, Y. Groysman, R. G. Jacobsen, R. W. Kadel, J. Kadyk, L. T. Kerth, Yu. G. Kolomensky, J. F. Kral, C. LeClerc, M. E. Levi, G. Lynch, L. M. Mir, P. J. Oddone, T. Orimoto, M. Pripstein, N. A. Roe, A. Romosan, M. T. Ronan, V. G. Shelkov, A. V. Telnov, W. A. Wenzel

Lawrence Berkeley National Laboratory and University of California, Berkeley, CA 94720, USA

T. J. Harrison, C. M. Hawkes, D. J. Knowles, S. W. O'Neale, R. C. Penny, A. T. Watson, N. K. Watson

University of Birmingham, Birmingham, B15 2TT, United Kingdom

T. Deppermann, K. Goetzen, H. Koch, B. Lewandowski, K. Peters, H. Schmuecker, M. Steinke

Ruhr Universität Bochum, Institut für Experimentalphysik 1, D-44780 Bochum, Germany

N. R. Barlow, W. Bhimji, J. T. Boyd, N. Chevalier, P. J. Clark, W. N. Cottingham, B. Foster, C. Mackay, F. F. Wilson

University of Bristol, Bristol BS8 1TL, United Kingdom

K. Abe, C. Hearty, T. S. Mattison, J. A. McKenna, D. Thiessen

University of British Columbia, Vancouver, BC, Canada V6T 1Z1

S. Jolly, A. K. McKemey

Brunel University, Uxbridge, Middlesex UB8 3PH, United Kingdom

V. E. Blinov, A. D. Bukin, A. R. Buzykaev, V. B. Golubev, V. N. Ivanchenko, A. A. Korol, E. A. Kravchenko, A. P. Onuchin, S. I. Serednyakov, Yu. I. Skovpen, A. N. Yushkov

Budker Institute of Nuclear Physics, Novosibirsk 630090, Russia

D. Best, M. Chao, D. Kirkby, A. J. Lankford, M. Mandelkern, S. McMahon, D. P. Stoker

University of California at Irvine, Irvine, CA 92697, USA

K. Arisaka, C. Buchanan, S. Chun

University of California at Los Angeles, Los Angeles, CA 90024, USA

D. B. MacFarlane, S. Prell, Sh. Rahatlou, G. Raven, V. Sharma

University of California at San Diego, La Jolla, CA 92093, USA

J. W. Berryhill, C. Campagnari, B. Dahmes, P. A. Hart, N. Kuznetsova, S. L. Levy, O. Long, A. Lu, M. A. Mazur, J. D. Richman, W. Verkerke

University of California at Santa Barbara, Santa Barbara, CA 93106, USA

J. Beringer, A. M. Eisner, M. Grothe, C. A. Heusch, W. S. Lockman, T. Pulliam, T. Schalk, R. E. Schmitz, B. A. Schumm, A. Seiden, M. Turri, W. Walkowiak, D. C. Williams, M. G. Wilson

University of California at Santa Cruz, Institute for Particle Physics, Santa Cruz, CA 95064, USA

E. Chen, G. P. Dubois-Felsmann, A. Dvoretskii, D. G. Hitlin, S. Metzler, J. Oyang, F. C. Porter, A. Ryd, A. Samuel, S. Yang, R. Y. Zhu

California Institute of Technology, Pasadena, CA 91125, USA

S. Jayatilleke, G. Mancinelli, B. T. Meadows, M. D. Sokoloff

University of Cincinnati, Cincinnati, OH 45221, USA

T. Barillari, P. Bloom, W. T. Ford, U. Nauenberg, A. Olivas, P. Rankin, J. Roy, J. G. Smith, W. C. van Hoek, L. Zhang

University of Colorado, Boulder, CO 80309, USA

J. Blouw, J. L. Harton, M. Krishnamurthy, A. Soffer, W. H. Toki, R. J. Wilson, J. Zhang

Colorado State University, Fort Collins, CO 80523, USA

T. Brandt, J. Brose, T. Colberg, M. Dickopp, R. S. Dubitzky, A. Hauke, E. Maly, R. Müller-Pfefferkorn, S. Otto, K. R. Schubert, R. Schwierz, B. Spaan, L. Wilden

Technische Universität Dresden, Institut für Kern- und Teilchenphysik, D-01062 Dresden, Germany

D. Bernard, G. R. Bonneaud, F. Brochard, J. Cohen-Tanugi, S. Ferrag, S. T'Jampens, Ch. Thiebaux, G. Vasileiadis, M. Verderi

Ecole Polytechnique, LLR, F-91128 Palaiseau, France

A. Anjomshoaa, R. Bernet, A. Khan, D. Lavin, F. Muheim, S. Playfer, J. E. Swain, J. Tinslay

University of Edinburgh, Edinburgh EH9 3JZ, United Kingdom

M. Falbo

Elon University, Elon University, NC 27244-2010, USA

C. Borean, C. Bozzi, L. Piemontese

Università di Ferrara, Dipartimento di Fisica and INFN, I-44100 Ferrara, Italy

E. Treadwell

Florida A&M University, Tallahassee, FL 32307, USA

F. Anulli,[1] R. Baldini-Ferroli, A. Calcaterra, R. de Sangro, D. Falciai, G. Finocchiaro, P. Patteri, I. M. Peruzzi,[2] M. Piccolo, Y. Xie, A. Zallo

Laboratori Nazionali di Frascati dell'INFN, I-00044 Frascati, Italy

S. Bagnasco, A. Buzzo, R. Contri, G. Crosetti, M. Lo Vetere, M. Macri, M. R. Monge, S. Passaggio, F. C. Pastore, C. Patrignani, E. Robutti, A. Santroni, S. Tosi

Università di Genova, Dipartimento di Fisica and INFN, I-16146 Genova, Italy

[1] Also with Università di Perugia, I-06100 Perugia, Italy
[2] Also with Università di Perugia, I-06100 Perugia, Italy

M. Morii
Harvard University, Cambridge, MA 02138, USA

R. Bartoldus, R. Hamilton, U. Mallik
University of Iowa, Iowa City, IA 52242, USA

J. Cochran, H. B. Crawley, J. Lamsa, W. T. Meyer, E. I. Rosenberg, J. Yi
Iowa State University, Ames, IA 50011-3160, USA

A. Höcker, H. M. Lacker, S. Laplace, F. Le Diberder, G. Grosdidier, V. Lepeltier, A. M. Lutz, S. Plaszczynski, M. H. Schune, S. Trincaz-Duvoid, G. Wormser
Laboratoire de l'Accélérateur Linéaire, F-91898 Orsay, France

R. M. Bionta, V. Brigljević , D. J. Lange, M. Mugge, K. van Bibber, D. M. Wright
Lawrence Livermore National Laboratory, Livermore, CA 94550, USA

A. J. Bevan, J. R. Fry, E. Gabathuler, R. Gamet, M. George, M. Kay, D. J. Payne, R. J. Sloane, C. Touramanis
University of Liverpool, Liverpool L69 3BX, United Kingdom

M. L. Aspinwall, D. A. Bowerman, P. D. Dauncey, U. Egede, I. Eschrich, G. W. Morton, J. A. Nash, P. Sanders, D. Smith, G. P. Taylor
University of London, Imperial College, London, SW7 2BW, United Kingdom

J. J. Back, G. Bellodi, P. Dixon, P. F. Harrison, R. J. L. Potter, H. W. Shorthouse, P. Strother, P. B. Vidal
Queen Mary, University of London, E1 4NS, United Kingdom

G. Cowan, H. U. Flaecher, S. George, M. G. Green, A. Kurup, C. E. Marker, T. R. McMahon, S. Ricciardi, F. Salvatore, G. Vaitsas, M. A. Winter
University of London, Royal Holloway and Bedford New College, Egham, Surrey TW20 0EX, United Kingdom

D. Brown, C. L. Davis
University of Louisville, Louisville, KY 40292, USA

J. Allison, R. J. Barlow, A. C. Forti, F. Jackson, G. D. Lafferty, N. Savvas, J. H. Weatherall, J. C. Williams
University of Manchester, Manchester M13 9PL, United Kingdom

A. Farbin, A. Jawahery, V. Lillard, J. Olsen, D. A. Roberts, J. R. Schieck
University of Maryland, College Park, MD 20742, USA

G. Blaylock, C. Dallapiccola, K. T. Flood, S. S. Hertzbach, R. Kofler, V. B. Koptchev, T. B. Moore, H. Staengle, S. Willocq
University of Massachusetts, Amherst, MA 01003, USA

B. Brau, R. Cowan, G. Sciolla, F. Taylor, R. K. Yamamoto
Massachusetts Institute of Technology, Laboratory for Nuclear Science, Cambridge, MA 02139, USA

M. Milek, P. M. Patel
McGill University, Montréal, QC, Canada H3A 2T8

F. Palombo

Università di Milano, Dipartimento di Fisica and INFN, I-20133 Milano, Italy

J. M. Bauer, L. Cremaldi, V. Eschenburg, R. Kroeger, J. Reidy, D. A. Sanders, D. J. Summers

University of Mississippi, University, MS 38677, USA

C. Hast, J. Y. Nief, P. Taras

Université de Montréal, Laboratoire René J. A. Lévesque, Montréal, QC, Canada H3C 3J7

H. Nicholson

Mount Holyoke College, South Hadley, MA 01075, USA

C. Cartaro, N. Cavallo, G. De Nardo, F. Fabozzi, C. Gatto, L. Lista, P. Paolucci, D. Piccolo, C. Sciacca

Università di Napoli Federico II, Dipartimento di Scienze Fisiche and INFN, I-80126, Napoli, Italy

J. M. LoSecco

University of Notre Dame, Notre Dame, IN 46556, USA

J. R. G. Alsmiller, T. A. Gabriel

Oak Ridge National Laboratory, Oak Ridge, TN 37831, USA

J. Brau, R. Frey, E. Grauges , M. Iwasaki, C. T. Potter, N. B. Sinev, D. Strom

University of Oregon, Eugene, OR 97403, USA

F. Colecchia, F. Dal Corso, A. Dorigo, F. Galeazzi, M. Margoni, M. Morandin, M. Posocco, M. Rotondo, F. Simonetto, R. Stroili, E. Torassa, C. Voci

Università di Padova, Dipartimento di Fisica and INFN, I-35131 Padova, Italy

M. Benayoun, H. Briand, J. Chauveau, P. David, Ch. de la Vaissière, L. Del Buono, O. Hamon, Ph. Leruste, J. Ocariz, M. Pivk, L. Roos, J. Stark

Universités Paris VI et VII, Lab de Physique Nucléaire H. E., F-75252 Paris, France

P. F. Manfredi, V. Re, V. Speziali

Università di Pavia, Dipartimento di Elettronica and INFN, I-27100 Pavia, Italy

E. D. Frank, L. Gladney, Q. H. Guo, J. Panetta

University of Pennsylvania, Philadelphia, PA 19104, USA

C. Angelini, G. Batignani, S. Bettarini, M. Bondioli, F. Bucci, G. Calderini, E. Campagna, M. Carpinelli, F. Forti, M. A. Giorgi, A. Lusiani, G. Marchiori, F. Martinez-Vidal, M. Morganti, N. Neri, E. Paoloni, M. Rama, G. Rizzo, F. Sandrelli, G. Triggiani, J. Walsh

Università di Pisa, Scuola Normale Superiore and INFN, I-56010 Pisa, Italy

M. Haire, D. Judd, K. Paick, L. Turnbull, D. E. Wagoner

Prairie View A&M University, Prairie View, TX 77446, USA

J. Albert, P. Elmer, C. Lu, V. Miftakov, S. F. Schaffner, A. J. S. Smith, A. Tumanov, E. W. Varnes

Princeton University, Princeton, NJ 08544, USA

F. Bellini, G. Cavoto, D. del Re, R. Faccini,[3] F. Ferrarotto, F. Ferroni, E. Leonardi, M. A. Mazzoni, S. Morganti, G. Piredda, F. Safai Tehrani, M. Serra, C. Voena

Università di Roma La Sapienza, Dipartimento di Fisica and INFN, I-00185 Roma, Italy

S. Christ, R. Waldi

Universität Rostock, D-18051 Rostock, Germany

T. Adye, N. De Groot, B. Franek, N. I. Geddes, G. P. Gopal, S. M. Xella

Rutherford Appleton Laboratory, Chilton, Didcot, Oxon, OX11 0QX, United Kingdom

R. Aleksan, S. Emery, A. Gaidot, P.-F. Giraud, G. Hamel de Monchenault, W. Kozanecki, M. Langer, G. W. London, B. Mayer, B. Serfass, G. Vasseur, Ch. Yèche, M. Zito

DAPNIA, Commissariat à l'Energie Atomique/Saclay, F-91191 Gif-sur-Yvette, France

M. V. Purohit, A. W. Weidemann, F. X. Yumiceva

University of South Carolina, Columbia, SC 29208, USA

I. Adam, D. Aston, N. Berger, A. M. Boyarski, M. R. Convery, D. P. Coupal, D. Dong, J. Dorfan, W. Dunwoodie, R. C. Field, T. Glanzman, S. J. Gowdy, T. Haas, T. Hadig, V. Halyo, T. Himel, T. Hryn'ova, M. E. Huffer, W. R. Innes, C. P. Jessop, M. H. Kelsey, P. Kim, M. L. Kocian, U. Langenegger, D. W. G. S. Leith, S. Luitz, V. Luth, H. L. Lynch, H. Marsiske, S. Menke, R. Messner, D. R. Muller, C. P. O'Grady, V. E. Ozcan, A. Perazzo, M. Perl, S. Petrak, H. Quinn, B. N. Ratcliff, S. H. Robertson, A. Roodman, A. A. Salnikov, T. Schietinger, R. H. Schindler, J. Schwiening, G. Simi, A. Snyder, A. Soha, S. M. Spanier, J. Stelzer, D. Su, M. K. Sullivan, H. A. Tanaka, J. Va'vra, S. R. Wagner, M. Weaver, A. J. R. Weinstein, W. J. Wisniewski, D. H. Wright, C. C. Young

Stanford Linear Accelerator Center, Stanford, CA 94309, USA

P. R. Burchat, C. H. Cheng, T. I. Meyer, C. Roat

Stanford University, Stanford, CA 94305-4060, USA

R. Henderson

TRIUMF, Vancouver, BC, Canada V6T 2A3

W. Bugg, H. Cohn

University of Tennessee, Knoxville, TN 37996, USA

J. M. Izen, I. Kitayama, X. C. Lou

University of Texas at Dallas, Richardson, TX 75083, USA

F. Bianchi, M. Bona, D. Gamba

Università di Torino, Dipartimento di Fisica Sperimentale and INFN, I-10125 Torino, Italy

L. Bosisio, G. Della Ricca, S. Dittongo, L. Lanceri, P. Poropat, L. Vitale, G. Vuagnin

Università di Trieste, Dipartimento di Fisica and INFN, I-34127 Trieste, Italy

R. S. Panvini

Vanderbilt University, Nashville, TN 37235, USA

[3] Also with University of California at San Diego, La Jolla, CA 92093, USA

C. M. Brown, D. Fortin, P. D. Jackson, R. Kowalewski, J. M. Roney
University of Victoria, Victoria, BC, Canada V8W 3P6

H. R. Band, S. Dasu, M. Datta, A. M. Eichenbaum, H. Hu, J. R. Johnson, R. Liu, F. Di Lodovico, Y. Pan, R. Prepost, I. J. Scott, S. J. Sekula, J. H. von Wimmersperg-Toeller, S. L. Wu, Z. Yu
University of Wisconsin, Madison, WI 53706, USA

T. M. B. Kordich, H. Neal
Yale University, New Haven, CT 06511, USA

1 Introduction

The study of charmless hadronic B decays is important to understand the phenomenon of CP violation in the Standard Model. There has been recent theoretical progress on using three-body decays to measure direct CP violation and to extract the Cabibbo-Kobayashi-Maskawa angle γ [1]. It is necessary to first observe these decays before such measurements can be made. We present updated preliminary results on the branching fractions of charged charmless three-body $B^{\pm} \rightarrow h^{\pm}h^{\mp}h^{\pm}$ decays, where $h = \pi$ or K, with no assumptions about intermediate resonances and with open charm contributions subtracted. Charge conjugate initial and final states are assumed throughout this document, unless stated otherwise.

2 The *BABAR* detector and dataset

The data used in this analysis were collected with the *BABAR* detector at the PEP-II asymmetric e^+e^- storage ring at SLAC. The data sample consists of 56.2 million $B\overline{B}$ pairs, corresponding to an integrated luminosity of 51.5 fb^{-1} collected at the $\Upsilon(4S)$ resonance (on-resonance) during the 2000-2001 run. In addition, a total integrated luminosity of 6.4 fb^{-1} was taken at 40 MeV below the $\Upsilon(4S)$ resonance (off-resonance), and was used to characterise the backgrounds from e^+e^- annihilation into light $q\overline{q}$ pairs.

The *BABAR* detector is described in detail elsewhere [2]; the main parts relevant for the analysis of three charged particle final states are the tracking and particle identification sub-detectors.

The 5-layer double-sided silicon vertex tracker (SVT) measures the impact parameters, angles, and transverse momenta of tracks down to 65 MeV/c. Outside the SVT is a 40-layer drift chamber (DCH) that measures the transverse momenta of tracks from their curvature in the 1.5-T solenoidal magnetic field. The SVT and DCH also are used to determine the mean ionisation energy loss of tracks to help identify charged particles. The tracking system has a momentum resolution of 0.5% for a transverse momentum of 1.0 GeV/c.

Surrounding the DCH is a detector of internally reflected Cherenkov radiation (DIRC), which provides charged hadron identification in the barrel region. Charged particles are identified by the Cherenkov angle θ_c and the number of photons measured with the DIRC. The typical separation between pions and kaons varies from $> 8\,\sigma$ at 2.0 GeV/c to 2.5σ at 4.0 GeV/c, where σ is the average resolution on θ_c. The kaon selection efficiency is approximately 80%, which is the product of the particle identification algorithm efficiency with geometrical acceptance, for a pion mis-identification probability of 2%.

The DIRC is surrounded by an electromagnetic calorimeter (EMC), made up of 6580 CsI(Tl) crystals, which is used to measure the energies and angular positions of photons and electrons with excellent resolution. The EMC is used to veto electrons in this analysis; the probability of mis-identifying electrons as pions is approximately 5%, while the probability of mis-identifying pions as electrons is below 0.3%.

3 Analysis method

The total branching fraction for each $B^{\pm} \rightarrow h^{\pm}h^{\mp}h^{\pm}$ mode is measured over the whole Dalitz plot - all resonant and non-resonant contributions are included. A set of selection criteria is applied to reconstruct each mode separately. Each Dalitz plot is divided into many equal area cells to enable us to find the selection efficiency as a function of position in the Dalitz plot. We also take into account continuum backgrounds and cross-feed between each signal mode from K and π mis-identification.

3.1 Candidate Selection

We reconstruct B candidates from charged tracks, where each track must have at least 12 hits in the DCH, a maximum momentum of 10 GeV/c, a minimum transverse momentum of 100 MeV/c, and must originate from the beam-spot. We find three-charged track combinations to form the B candidates, and we require that their energies and momenta satisfy kinematic constraints appropriate for B mesons.

There are two variables we use for this, the first of which is the beam-energy substituted mass $m_{\mathrm{ES}} = \sqrt{(E_b^2 - \mathbf{p}_B^2)}$. The energy of the B candidate is defined as $E_b = (\frac{1}{2}s + \mathbf{p}_0 \cdot \mathbf{p}_B)/E_0$, where $\sqrt{s}$ and E_0 are the total energies of the e^+e^- system in the centre-of-mass (CM) and laboratory frames, respectively, and $\mathbf{p}_0$ and $\mathbf{p}_B$ are the momentum vectors in the laboratory frame of the e^+e^- system and the B candidate, respectively. The m_{ES} value should be close to the nominal B mass for signal events.

The second variable we use is the energy difference between the reconstructed B candidate energy and the beam energy, $\Delta E = E_B^* - \sqrt{s}/2$, where E_B^* is the energy of the B candidate in the CM system. For this analysis, we assume the appropriate mass hypothesis for each charged track in a given decay mode under study in calculating ΔE. For signal events, ΔE should be centred at zero. The typical ΔE separation between modes that differ by substituting a kaon for a pion in the final state is 45 MeV.

We use dE/dx information from the SVT and DCH, and the Cherenkov angle and number of photons measured by the DIRC for tracks with momenta above 700 MeV/c, to identify charged pions and kaons. Kaons are selected with requirements made to the product of the likelihood ratios determined from these measurements. The likelihood ratio requirements are established by requiring the probability of mis-identifying pions as kaons be below 5%, up to a momentum of 4.0 GeV/c. Pions are required to fail the kaon selection. We veto electron candidates by requiring that they fail a selection based on information from dE/dx, shower shapes in the EMC and the ratio of the shower energy and track momentum.

Since we are only interested in charmless decays, we need to veto candidates that contain charm mesons. We remove B candidates when the invariant mass of the combination of any two of its daughter tracks (of opposite charge) is within 3 σ of the mass of D^0, J/ψ or $\psi(2S)$ mesons. Here, σ is 10.0 MeV/c^2 for D^0 and 15.0 MeV/c^2 for J/ψ and $\psi(2S)$. All possible kaon and pion combinations are tested for the D^0 veto, while only the K^+K^- and $\pi^+\pi^-$ hypotheses are tested for the J/ψ and $\psi(2S)$ vetoes, since the background from these decays is from leptonic decays, in which the leptons have been mis-identified as pions or kaons. The electron veto helps to reduce the combinatorial background from J/ψ and $\psi(2S)$ decays that would otherwise pass the 3 σ invariant mass veto.

3.2 Background Suppression and Characterisation

In addition to these candidate selection requirements, we need to suppress backgrounds from light quark and charm continuum production. We reduce these by imposing requirements on two topological event shape variables computed in the $\Upsilon(4S)$ rest frame.

The first event shape variable is the cosine of the angle θ_T between the thrust axis of the selected B candidate and the thrust axis of the rest of the event, i.e. all charged tracks and neutral particles not in the B meson candidate. For continuum backgrounds, the directions of the two axes tend to be aligned because the daughters of the reconstructed candidate generally lie along the dijet axis of such events. Therefore, the distribution of $|\cos\theta_T|$ is strongly peaked towards unity. For B events, the distribution of $|\cos\theta_T|$ is isotropic because the decay products from the two B mesons are essentially independent of each other. The difference in the $|\cos\theta_T|$ dependence allows us to discriminate between signal B decays and continuum background.

The second event shape variable is a Fisher discriminant [3] $\mathcal{F}$, which is formed from the linear combination

$$\mathcal{F} = \sum_{i=1}^{9} \alpha_i x_i \tag{1}$$

of the input variables x_i. The available variables are the summed scalar momenta of all charged and neutral particles from the rest of the event within nine nested cones coaxial with the thrust axis of the B candidate. The coefficients α_i are chosen to maximise the separation between signal and background events. They are calculated for each signal mode separately using Monte Carlo signal and light quark continuum events.

Figure 1 shows the Fisher distributions for $\Upsilon(4S)$ events, from the control sample $B^- \to D^0\pi^-, D^0 \to K^-\pi^+$ in Monte Carlo simulation and on-resonance data, and for background, from off-resonance data and light-quark continuum Monte Carlo events.

The selection criteria for the event shape variables, shown in Table 1, is optimised separately for each signal mode to achieve maximum sensitivity for the branching fraction.

Table 1: Selection requirements on the event shape variables for each signal mode.

Signal Mode	$\|\cos\theta_T\|$	$\mathcal{F}$
$\pi^\pm\pi^\mp\pi^\pm$	< 0.575	< -0.11
$K^\pm\pi^\mp\pi^\pm$	< 0.700	< -0.03
$K^\pm K^\mp\pi^\pm$	< 0.725	< 0.10
$K^\pm K^\mp K^\pm$	< 0.875	< 0.30

Despite using the powerful event shape variables mentioned above, there are still significant backgrounds that must be explicitly subtracted to extract a signal. The residual background level is estimated from the observed number of events in a sideband region, located near to the signal region in the m_{ES}- ΔE plane, and then extrapolating into the signal region by using a multiplicative factor, R. We define R to be the ratio of the number of background candidates in the signal region to the number in the sideband region. In order to determine R, the shape of the background distribution as a function of m_{ES} is parameterised according to the ARGUS function [4], and is measured using the upper sideband in the ΔE variable in on-resonance data ($0.1 < |\Delta E| < 0.25\,\mathrm{GeV}$). A quadratic function is used to parameterise the background distribution as a function of ΔE. The ratio of the areas under the shape function in ΔE and m_{ES} in the signal and sideband regions is equal to R. The uncertainty of the value of R is dominated by the uncertainty of the shape parameter for the ARGUS function. Off-resonance data give a consistent value of R.

3.3 Branching Fraction Calculation

As mentioned previously, the branching fractions for each signal mode are measured over the whole Dalitz plot, and each Dalitz plot is divided up into many cells so that the bin-by-bin variation of the selection efficiency can be found for each plot.

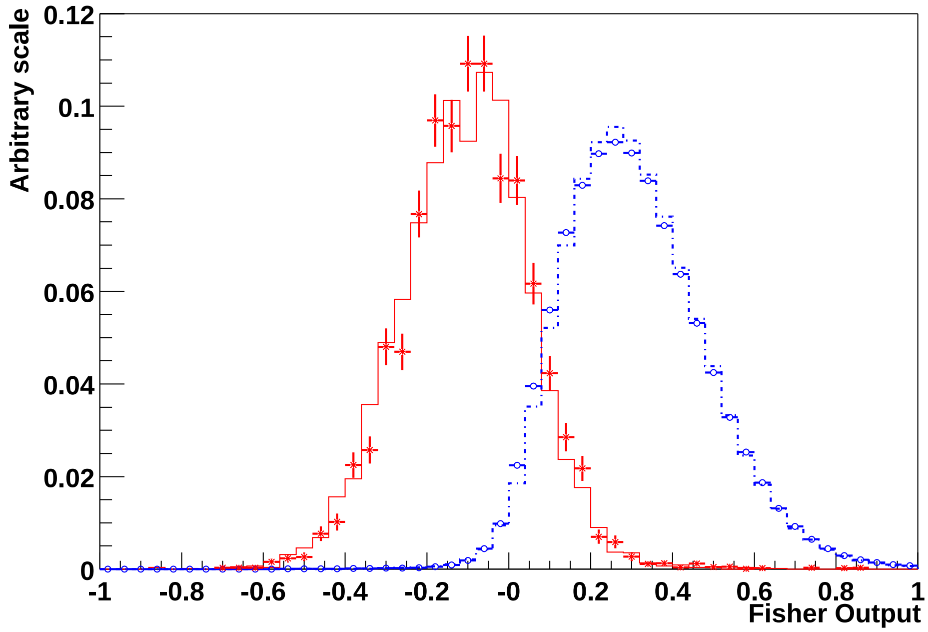

Figure 1: Normalised distributions of the Fisher discriminant for $B^- \to D^0\pi^-, D^0 \to K^-\pi^+$ Monte Carlo events (solid histogram), on-resonance $D^0\pi^-$ data (solid points), light quark continuum Monte Carlo events (dotted histogram) and off-resonance data (dotted points).

Taking ϵ_i to be the Monte Carlo efficiency of reconstructing the signal in the i^{th} bin in the Dalitz plot, the branching fraction for the signal mode is given by:

$$\mathcal{B} = \frac{1}{N_{B\overline{B}}} \sum_i \frac{(N_{1i} - RN_{2i})}{\epsilon_i} = \frac{1}{N_{B\overline{B}}} \sum_i \frac{S_i}{\epsilon_i}, \tag{2}$$

where $N_{B\overline{B}}$ is the total number of $B\overline{B}$ pairs, R is the background extrapolation factor into the signal region, and N_{1i} and N_{2i} are the number of events observed in the signal and grand sideband (GSB) regions, respectively, for the i^{th} Dalitz plot bin. No significant differences were found for the value of R in different regions of the Dalitz plot, so an average value is used for all bins. S_i is the number of background subtracted signal events for the i^{th} Dalitz plot bin.

The signal region is defined to be $|m_{\mathrm{ES}} - m_B| < 8.0$ MeV$/c^2$ and $|\Delta E - \langle\Delta E\rangle| < 60.0$ MeV, where $\langle\Delta E\rangle$ is the mean value of ΔE for on-resonance data for the calibration sample $B^- \to D^0\pi^-, D^0 \to K^-\pi^+$, and m_B is the nominal mass of the charged B meson [5]. The GSB region is defined to be $5.21 < m_{\mathrm{ES}} < 5.25$ GeV$/c^2$ and $|\Delta E - \langle\Delta E\rangle| < 100.0$ MeV.

The probability of a kaon being mis-identified as a pion is 20%, which includes the efficiency of the particle identification algorithm and the geometrical acceptance. This means that there is significant cross-feed into the signal region from the decay mode that has one more kaon, which must be subtracted for each bin, i. To see how this is done, consider the branching fraction calculation for $B^\pm \to K^\pm K^\mp K^\pm$. This channel has negligible cross-feed from the other modes, so we have

$$\mathcal{B}(B^\pm \to K^\pm K^\mp K^\pm) = \frac{1}{N_{B\overline{B}}} \sum_i \frac{S_i}{\epsilon_i} = \frac{N_{3K}}{N_{B\overline{B}}}, \tag{3}$$

where N_{3K} is the total number of $B^\pm \to K^\pm K^\mp K^\pm$ events in the data. The channel $K^\pm K^\mp \pi^\pm$, on the other hand, has significant cross-feed from $K^\pm K^\mp K^\pm$, and this must be subtracted from the signal. The branching fraction for this mode is given by

$$\mathcal{B}(B^\pm \to K^\pm K^\mp \pi^\pm) = \frac{1}{N_{B\overline{B}}} \sum_i \frac{(S_i - N_{3K}\epsilon_i'')}{\epsilon_i} = \frac{N_{KK\pi}}{N_{B\overline{B}}}, \tag{4}$$

where $N_{KK\pi}$ is the total number of $B^\pm \to K^\pm K^\mp \pi^\pm$ events in the data, and S_i and ϵ_i refer to those quantities for $B^\pm \to K^\pm K^\mp \pi^\pm$. Here, ϵ_i'' is the probability for reconstructing $B^\pm \to K^\pm K^\mp K^\pm$ events using the selection criteria for $B^\pm \to K^\pm K^\mp \pi^\pm$. It is determined from Monte Carlo simulation by generating events uniformly in phase space and determining the cross-feed selection efficiency in each Dalitz plot bin.

The branching fraction for $B^\pm \to K^\pm \pi^\mp \pi^\pm$ is given by

$$\mathcal{B}(B^\pm \to K^\pm \pi^\mp \pi^\pm) = \frac{1}{N_{B\overline{B}}} \sum_i \frac{(S_i - N_{KK\pi}\epsilon_i'' - n_{Di})}{\epsilon_i} = \frac{N_{K\pi\pi}}{N_{B\overline{B}}}, \tag{5}$$

where $N_{K\pi\pi}$ is the total number of $B^\pm \to K^\pm \pi^\mp \pi^\pm$ events in the data, and S_i and ϵ_i refer to the number of background subtracted events in the signal region and selection efficiency for $B^\pm \to K^\pm \pi^\mp \pi^\pm$, respectively. Here, ϵ_i'' is the probability for reconstructing $B^\pm \to K^\pm K^\mp \pi^\pm$ events using the selection criteria for $B^\pm \to K^\pm \pi^\mp \pi^\pm$. This channel has some D^0 contamination from candidates falling outside the 3 σ invariant mass veto, which must be subtracted. This is represented by the term n_{Di}, which is the number of D^0 events that is expected to populate the i^{th} bin in the Dalitz plot. This is estimated by finding the probability of reconstructing D^0 Monte Carlo events, for each bin i, using the selection criteria for $B^\pm \to K^\pm \pi^\mp \pi^\pm$, and multiplying this by the measured branching fraction for the D^0 mode [5] and the total number of $B\overline{B}$ pairs, $N_{B\overline{B}}$. The total expected number of $B^- \to D^0\pi^-, D^0 \to K^-\pi^+$ events that must be subtracted across the full Dalitz plot for this channel is 47 ± 8. The values of n_{Di} are non-zero only for bins close to the D^0 resonance bands.

Finally, the branching fraction for $B^\pm \to \pi^\pm \pi^\mp \pi^\pm$ is given by

$$\mathcal{B}(B^\pm \to \pi^\pm \pi^\mp \pi^\pm) = \frac{1}{N_{B\overline{B}}} \sum_i \frac{(S_i - N_{K\pi\pi}\epsilon_i'' - n_{Di})}{\epsilon_i} = \frac{N_{3\pi}}{N_{B\overline{B}}}, \tag{6}$$

where $N_{3\pi}$ is the total number of $B^\pm \to \pi^\pm \pi^\mp \pi^\pm$ events in the data, ϵ_i'' is the probability for reconstructing $B^\pm \to K^\pm \pi^\mp \pi^\pm$ events using the selection criteria for $B^\pm \to \pi^\pm \pi^\mp \pi^\pm$, and S_i and ϵ_i refer to the number of background subtracted events in the signal region and selection efficiency for $B^\pm \to \pi^\pm \pi^\mp \pi^\pm$, respectively. Again, there are some $B^- \to D^0\pi^-, D^0 \to K^-\pi^+$ events (23 ± 5) that pass the selection criteria for this channel, because the kaon from the D^0 decay is mis-identified as a pion, and where the invariant mass of the D^0 meson lies outside the 3 σ invariant mass window. This background is subtracted from the signal.

In addition to the cross-feed where only one of the kaon tracks is mis-identified as a pion, there can also be cross-feed where either two kaons are mis-identified as pions (probability of 4%) or when one of the pions is mis-identified as a kaon (probability of 2%). These are smaller, second-order cross-feed effects, and so it is adequate to subtract the average number of events over the whole Dalitz plot. If n_x is the average number of second-order cross-feed events that has to be subtracted (i.e. the number of events reconstructed divided by the appropriate cross-feed efficiency), then we finally have

$$\mathcal{B} = \frac{1}{N_{B\overline{B}}}\left(\sum_i \frac{(S_i - N_x\epsilon_i'' - n_{Di})}{\epsilon_i} - n_x\right), \tag{7}$$

where N_x is the total number of events from the channel that contributes to most of the (first-order) cross-feed, e.g. $N_x = N_{K\pi\pi}$ for $B^\pm \to \pi^\pm\pi^\mp\pi^\pm$.

Table 2: Efficiencies and cross-contamination probabilities between the signal modes derived from Monte Carlo samples. For example, the probability that an event $K^\pm\pi^\mp\pi^\pm$ will be reconstructed as $\pi^\pm\pi^\mp\pi^\pm$ is $(1.7 \pm 0.1) \times 10^{-2}$.

Selection Criteria Hypothesis	Input Decay Mode			
	$\pi^\pm\pi^\mp\pi^\pm$	$K^\pm\pi^\mp\pi^\pm$	$K^\pm K^\mp\pi^\pm$	$K^\pm K^\mp K^\pm$
$\pi^\pm\pi^\mp\pi^\pm$	$(15.3 \pm 0.2) \times 10^{-2}$	$(1.7 \pm 0.1) \times 10^{-2}$	$(1.4 \pm 0.9) \times 10^{-4}$	$(1.1 \pm 3.2) \times 10^{-5}$
$K^\pm\pi^\mp\pi^\pm$	$(3.6 \pm 0.4) \times 10^{-3}$	$(15.1 \pm 0.2) \times 10^{-2}$	$(3.2 \pm 0.2) \times 10^{-2}$	$(4.0 \pm 1.7) \times 10^{-4}$
$K^\pm K^\mp\pi^\pm$	$(0.0 \pm 0.2) \times 10^{-3}$	$(2.9 \pm 0.4) \times 10^{-3}$	$(17.7 \pm 0.3) \times 10^{-2}$	$(5.5 \pm 0.2) \times 10^{-2}$
$K^\pm K^\mp K^\pm$	$(0.0 \pm 0.2) \times 10^{-3}$	$(0.0 \pm 0.2) \times 10^{-3}$	$(1.7 \pm 0.2) \times 10^{-3}$	$(21.6 \pm 0.3) \times 10^{-2}$

The Dalitz plot for each signal mode is divided into cells with equal area 1.0 GeV^4, and large samples of Monte Carlo signal events are used to obtain the signal and cross-feed selection efficiencies across each Dalitz plot. Table 2 shows the signal and cross-feed selection efficiencies for the modes, averaged over the Dalitz plots.

4 Experimental Uncertainties

There are several sources of uncertainty for the branching fraction measurements, which come from the various terms in Eq. 7. The statistical uncertainties come from the number of events observed in the signal and GSB regions, N_1 and N_2. The factor R, found independently for each mode, has a systematic uncertainty arising from the uncertainty in the fitted ARGUS shape parameter, ξ. The main sources of B-related background are D^0 decays (the n_{Di} term) and cross-feed from the other signal modes (the N_x and n_x terms), owing to kaon and pion mis-identification. We deal with these by explicitly subtracting them from the signal. The uncertainty in the number of D^0 events that have to be subtracted comes from the uncertainty on the published measured branching fractions [5], the number of $B\overline{B}$ events (mentioned below) and the selection efficiency.

Since there are a lot of terms used to calculate the branching fraction, it is worthwhile to go through what uncertainties they contribute to the end result. If we let X_i represent the term within parenthesis in Eq. 7, then the fractional uncertainty on the branching fraction is

$$\left(\frac{\Delta\mathcal{B}}{\mathcal{B}}\right)^2 = \left(\frac{\Delta N_{B\overline{B}}}{N_{B\overline{B}}}\right)^2 + \left(\frac{\Delta(\sum_i X_i)}{(\sum_i X_i)}\right)^2 + \delta_e^2, \tag{8}$$

where δ_e is the fractional systematic error for the efficiency that comes from differences between Monte Carlo simulation and on-resonance data, shown in Table 3. Going through the terms for X_i, we have

$$\left(\Delta(\sum_i X_i)\right)^2 = \sum_i \frac{N_{1i}}{\epsilon_i^2} + R^2 \sum_i \frac{N_{2i}}{\epsilon_i^2} + (\Delta R)^2 \left(\sum_i \frac{N_{2i}}{\epsilon_i}\right)^2$$
$$+N_x^2 \sum_i \left(\frac{\Delta\epsilon_i''}{\epsilon_i}\right)^2 + (\Delta N_x)^2 \left(\sum_i \frac{\epsilon_i''}{\epsilon_i}\right)^2 + \sum_i \left(\frac{\Delta n_{Di}}{\epsilon_i}\right)^2$$
$$+\sum_i \left(\Delta\epsilon_i \frac{N_{1i} - RN_{2i} - N_x\epsilon_i'' - n_{Di}}{\epsilon_i^2}\right)^2 + (\Delta n_x)^2. \quad (9)$$

The first two terms on the right hand side (R.H.S.) are the statistical uncertainties on the number of events in the signal and GSB regions, while the third term represents the systematic variation for the background extrapolation factor, R. The uncertainties from the cross-feed subtraction are represented by the next three terms, while the penultimate term is that for the bin-by-bin uncertainty for the efficiency. The last term is the uncertainty for the number of second-order cross-feed events. The various sources of error mentioned above will be shown in detail for each branching fraction result.

The uncertainties on the signal efficiencies and cross-feed probabilities are the combination of statistical errors on the number of events selected in the Monte Carlo samples relative to the total number generated, as well as systematic uncertainties arising from the difference between Monte Carlo simulation and on-resonance data.

The average fractional Monte Carlo statistical uncertainties of the signal efficiencies per Dalitz plot bin ($\Delta\epsilon_i/\epsilon_i$) are 7.0% for $\pi^\pm\pi^\mp\pi^\pm$, 9.1% for $K^\pm\pi^\mp\pi^\pm$, 9.5% for $K^\pm K^\mp\pi^\pm$ and 7.4% for $K^\pm K^\mp K^\pm$.

The Monte Carlo simulation is subject to systematic uncertainties from tracking and particle identification efficiencies. Residual differences in the tracking selection efficiencies between on-resonance data and Monte Carlo simulation contributes a fractional uncertainty of 0.8% on the efficiency per track. This uncertainty is added coherently for all three tracks used to reconstruct each B meson. Both the electron veto and kaon selections have fractional systematic uncertainties of 1.0%. These uncertainties are added coherently.

Possible differences between the behaviour of Monte Carlo simulation and on-resonance data are also examined for the Fisher distributions used to discriminate signal B decays from light quark continuum events. The control samples $B^- \to D^0 h^-, D^0 \to h^- h^+$, where $h = \pi$ and/or K, which have similar kinematics to the signal modes, are used to compare the signal Fisher distributions between on-resonance and Monte Carlo data, using the Fisher coefficients derived from Monte Carlo signal and $q\overline{q}$ samples. The choice for h is made such that the final state of the control sample decay has the same number of kaons and pions as those for the signal mode.

The Fisher distribution for off-resonance data agrees with that for light quark continuum Monte Carlo events, which can be seen in Fig. 1. There are very slight differences between the Fisher distributions for Monte Carlo signal events and on-resonance data. To quantify this difference, the Fisher distributions are fitted to double Gaussian functions. The differences in the mean and width values between on-resonance and Monte Carlo $D^0 h$ events are used to shift and scale the Fisher distributions for the signal Monte Carlo modes. The change in the selection efficiency gives an estimate of the correction factor necessary for the requirement on the Fisher variable used in the selection for each mode, which is found to be very small (approximately 1%). The systematic uncertainty on this correction is found by varying the parameters of the Fisher distribution for the signal Mode Carlo modes by the (scaled) uncertainties found for the fitted parameters for the D^0 control sample.

The resolutions for ΔE and $m_{\rm ES}$ in data differ by a negligible amount from Monte Carlo predictions. The main source of uncertainty arises from a +7 MeV shift in the mean value of ΔE observed in the control sample $B^- \to D^0\pi^-, D^0 \to K^-\pi^+$ in on-resonance data, which we correct for in the Monte Carlo. This contributes a fractional systematic uncertainty of 1%.

Table 3 gives a summary of the systematic uncertainties to the efficiency for each mode (not including the Dalitz plot variation). The fractional uncertainties for the Dalitz plot variation for the cross-feed probabilities ($\Delta\epsilon''_i/\epsilon''_i$) are approximately 30%.

Table 3: Fractional systematic uncertainties for the Monte Carlo efficiency for each signal mode. The uncertainties are added in quadrature in the total.

Source of Uncertainty	Fractional error on efficiency (%)			
	$\pi^\pm\pi^\mp\pi^\pm$	$K^\pm\pi^\mp\pi^\pm$	$K^\pm K^\mp\pi^\pm$	$K^\pm K^\mp K^\pm$
Tracking	2.4	2.4	2.4	2.4
Fisher Discriminant	2.1	0.7	0.5	1.7
Particle Identification	6.0	5.0	4.0	3.0
ΔE and $m_{\rm ES}$	1.0	1.0	1.0	1.0
Total	6.8	5.6	4.7	4.2

Finally, there is a systematic uncertainty on the overall normalisation, $N_{B\overline{B}}$, which is obtained from a dedicated study to find the number of B mesons produced in the data sample. This is found to have a systematic uncertainty of 1.5%.

5 Physics results

Our preliminary measurements of the branching fractions for the signal modes are summarised in Table 4. The top few rows of this table show the total number of events observed in the signal and GSB regions, as well as the average signal reconstruction efficiencies for each mode and the values of the background extrapolation factor R.

The row labelled 1) shows the sum over Dalitz plot bins of the number of events observed in the signal region divided by the signal efficiency. The error on these quantities is the first error shown in Eq. 9, and only includes the uncertainty in the number of signal events, N_{1i}.

The next row, labelled 2), shows the sum over Dalitz plot bins of the expected number of background events divided by the signal efficiency. The errors shown for these values are the second and third terms on the R.H.S. of Eq. 9, respectively. They correspond to the statistical uncertainty in N_{2i}, and the systematic error for R, which is dominant.

Row 3) shows the expected number of cross-feed events (from K/π mis-identification). The errors on these quantities represent the fourth and fifth terms on the R.H.S. of Eq. 9 only. Note that the $B^\pm \to K^\pm K^\mp K^\pm$ mode does not have a cross-feed term, since this is negligible.

The expected number of D^0 events passing the selection criteria for $B^\pm \to \pi^\pm\pi^\mp\pi^\pm$ and $B^\pm \to K^\pm\pi^\mp\pi^\pm$ is shown in row 4), where the error for each value is the sixth term on the R.H.S. of Eq. 9.

The second-order cross-feed terms, n_x, are shown in row 5). There are only entries for $B^\pm \to K^\pm\pi^\mp\pi^\pm$, from $B^\pm \to K^\pm K^\mp K^\pm$ events, and for $B^\pm \to K^\pm K^\mp\pi^\pm$, from $B^\pm \to K^\pm\pi^\mp\pi^\pm$ cross-feed. The errors for these values are dominated by the uncertainties in the second-order cross-feed probabilities. Note that the n_x term for $B^\pm \to K^\pm\pi^\mp\pi^\pm$ is negative, which compensates for the extra cross-feed background of $B^\pm \to K^\pm K^\mp K^\pm$ events that is mis-identified as $B^\pm \to K^\pm K^\mp \pi^\pm$, and then in turn passes the selection criteria for $B^\pm \to K^\pm\pi^\mp\pi^\pm$.

The various contributions to the signal and background terms are shown in row 6). The first uncertainties are the combination of the statistical errors for the number of events in the signal and GSB regions - they correspond to the sum in quadrature of the error for row 1), and the first error in row 2). The second error for the entries in row 6) corresponds to the quadrature sum of all the other systematic errors from rows 2) to 5). The third error for row 6) is that from the penultimate term on the R.H.S. of Eq. 9, i.e. the uncertainty for the selection efficiency for each of the Dalitz plot bins separately (not the average). The last error for row 6) is just the fractional systematic uncertainty for the efficiency correction factors, given in Table 3.

The last row in Table 4 shows the branching fraction results, where the first uncertainties are the statistical errors on the number of signal and background events, while the second uncertainties are the sum in quadrature of all systematic errors. The dominant systematic uncertainty for $B^\pm \to K^\pm K^\mp K^\pm$ is the systematic correction factor for the efficiency, while for $B^\pm \to \pi^\pm\pi^\mp\pi^\pm$ and $B^\pm \to K^\pm K^\mp \pi^\pm$, the background extrapolation factor R dominates. For $B^\pm \to K^\pm\pi^\mp\pi^\pm$, both uncertainties contribute equally to the systematic error.

As a consistency check, the branching fraction for the control sample $B^- \to D^0\pi^-$, $D^0 \to K^-\pi^+$ is measured to be $(180 \pm 4 \pm 11) \times 10^{-6}$, which agrees with the previously measured value of $(203 \pm 20) \times 10^{-6}$ [5].

Figures 2 to 5 show the ΔE and $m_{\rm ES}$ distributions for the signal region for each of the modes. Each plot shows the expected levels continuum and $B\overline{B}$ background (solid and dashed lines, respectively).

Figures 6 to 9 show the unbinned Dalitz plots for the signal modes in the GSB and signal regions, where no efficiency corrections have been applied. Only the upper half of the symmetrical Dalitz plot is shown for the $B^\pm \to \pi^\pm\pi^\mp\pi^\pm$ and $B^\pm \to K^\pm K^\mp K^\pm$ channels, where the x and y axes show the minimum and maximum values of the Dalitz plot variables, respectively.

There are clear signals for the modes $B^\pm \to K^\pm\pi^\mp\pi^\pm$ and $B^\pm \to K^\pm K^\mp K^\pm$. No signal is observed for $B^\pm \to K^\pm K^\mp \pi^\pm$, and the result for $B^\pm \to \pi^\pm\pi^\mp\pi^\pm$ is interpreted as an upper limit on the branching fraction, although there is a positive excess of signal events with 2.2 σ significance. Since there are a large number of events in the selected samples, we can assume that the number of signal and background events observed in the signal region are Gaussian distributed. The 90% C.L. upper limits are computed using the standard prescription for a one-sided confidence interval from a Gaussian distributed measurement, i.e.,

$$\mathcal{B}_{UL} = \mathcal{B} + 1.28\Delta\mathcal{B}, \tag{10}$$

where $\mathcal{B}$ is the estimated branching ratio and $\Delta\mathcal{B}$ is its standard deviation. Here, however, we take $\Delta\mathcal{B}$ to be the total error (quadratic sum of statistical and systematic uncertainties).

Table 4: Branching fraction results for on-resonance data. The uncertainties for each term are explained in the text.

Signal Mode	$\pi^{\pm}\pi^{\mp}\pi^{\pm}$	$K^{\pm}\pi^{\mp}\pi^{\pm}$	$K^{\pm}K^{\mp}\pi^{\pm}$	$K^{\pm}K^{\mp}K^{\pm}$
No. of events in signal region, $\sum_i N_{1i}$	951	1269	573	603
No. of events in GSB, $\sum_i N_{2i}$	5470	4652	3239	1100
Average signal efficiency (%)	15.3 ± 1.1	15.4 ± 0.9	18.3 ± 0.9	22.5 ± 1.0
Background factor, R	0.145 ± 0.006	0.153 ± 0.006	0.150 ± 0.006	0.159 ± 0.010
1) $\sum_i N_{1i}/\epsilon_i$	5839 ± 212	8055 ± 255	3414 ± 156	2734 ± 111
2) $\sum_i RN_{2i}/\epsilon_i$	$4812 \pm 73 \pm 193$	$4434 \pm 73 \pm 171$	$2802 \pm 54 \pm 111$	$780 \pm 23 \pm 47$
3) $\sum_i N_x\epsilon_i''/\epsilon_i$	$391 \pm 8 \pm 2$	$14 \pm 1 \pm 1$	$435 \pm 5 \pm 7$	—
4) No. of D^0 events, $\sum_i n_{Di}/\epsilon_i$	157 ± 27	401 ± 50	—	—
5) 2^{nd}-order cross-feed, n_x	—	-122 ± 54	57 ± 11	—
6) $\sum_i \frac{(N_{1i}-RN_{2i}-N_x\epsilon_i''-n_{Di})}{\epsilon_i} - n_x$	$478 \pm 224 \pm 195$ $\pm 34 \pm 33$	$3328 \pm 266 \pm 186$ $\pm 56 \pm 186$	$120 \pm 166 \pm 112$ $\pm 22 \pm 6$	$1954 \pm 114 \pm 47$ $\pm 13 \pm 82$
Branching Fraction ($\times 10^{-6}$) Statistical Significance (σ) 90% Upper Limit ($\times 10^{-6}$)	$8.5 \pm 4.0 \pm 3.6$ 2.2 < 15	$59.2 \pm 4.7 \pm 4.9$ > 6	$2.1 \pm 2.9 \pm 2.0$ 0.9 < 7	$34.7 \pm 2.0 \pm 1.8$ > 6

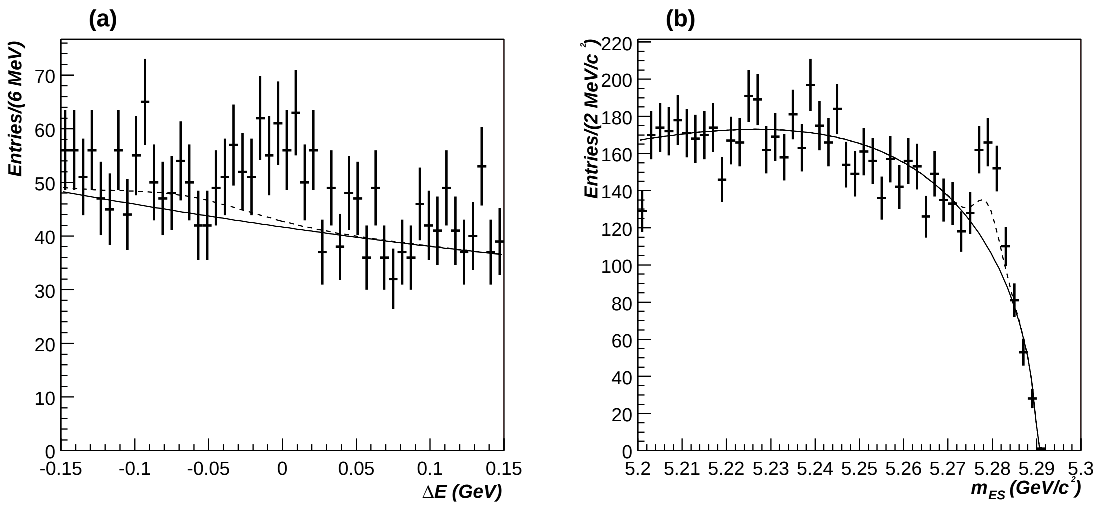

Figure 2: On-resonance signal region ΔE (a) and $m_{\rm ES}$ (b) distributions for $B^{\pm} \rightarrow \pi^{\pm}\pi^{\mp}\pi^{\pm}$. The solid lines show the expected level of continuum background, using appropriately normalised background shapes from the sideband regions in on-resonance data. The dotted lines show the expected level of $B\overline{B}$ background, which is obtained from the sum of Gaussian distributions from Monte Carlo estimated cross-feed and $D^0\pi$ events, each normalised to the number of events observed in on-resonance data that passed the selection criteria for $B^{\pm} \rightarrow \pi^{\pm}\pi^{\mp}\pi^{\pm}$.

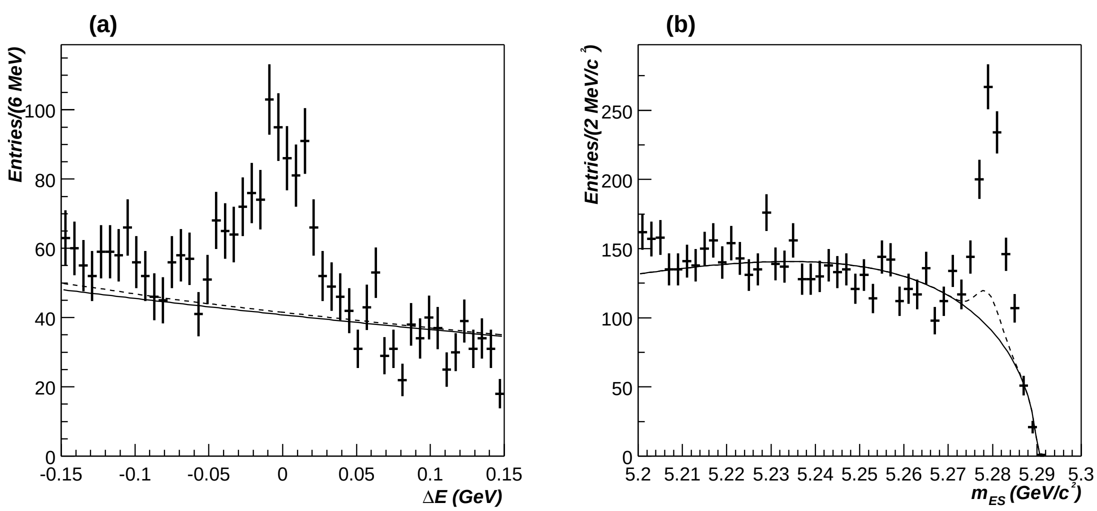

Figure 3: On-resonance signal region ΔE (a) and $m_{\rm ES}$ (b) distributions for $B^{\pm} \rightarrow K^{\pm}\pi^{\mp}\pi^{\pm}$. The solid lines show the expected level of continuum background, using appropriately normalised background shapes from the sideband regions in on-resonance data. The dotted lines show the expected level of $B\overline{B}$ background, which is obtained from the sum of Gaussian distributions from Monte Carlo estimated cross-feed and $D^0\pi$ events, each normalised to the number of events observed in on-resonance data that passed the selection criteria for $B^{\pm} \rightarrow K^{\pm}\pi^{\mp}\pi^{\pm}$.

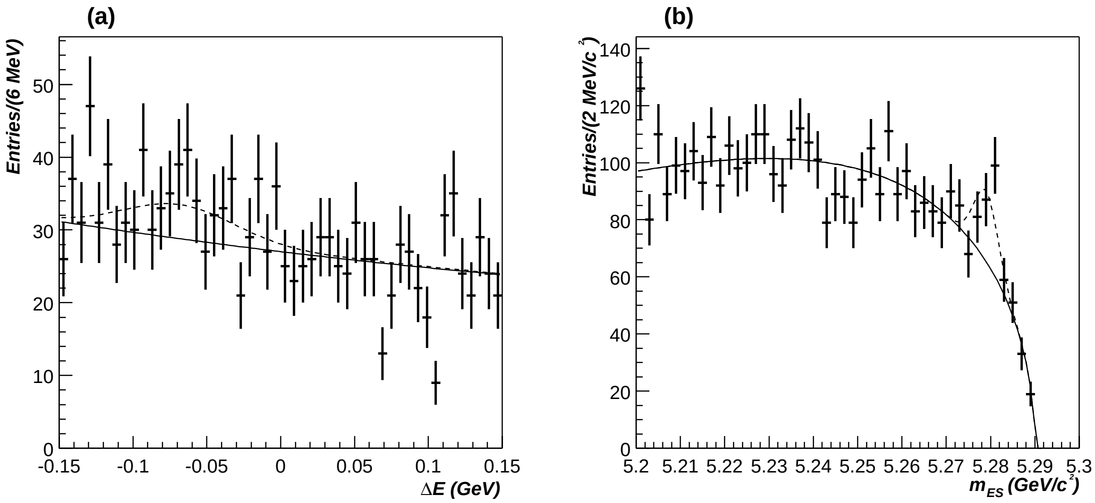

Figure 4: On-resonance signal region ΔE (a) and $m_{\rm ES}$ (b) distributions for $B^{\pm} \rightarrow K^{\pm}K^{\mp}\pi^{\pm}$. The solid lines show the expected level of continuum background, using appropriately normalised background shapes from the sideband regions in on-resonance data. The dotted lines show the expected level of $B\overline{B}$ background, which is obtained from the sum of Gaussian distributions from Monte Carlo estimated cross-feed events, each normalised to the number of events observed in on-resonance data that passed the selection criteria for $B^{\pm} \rightarrow K^{\pm}K^{\mp}\pi^{\pm}$.

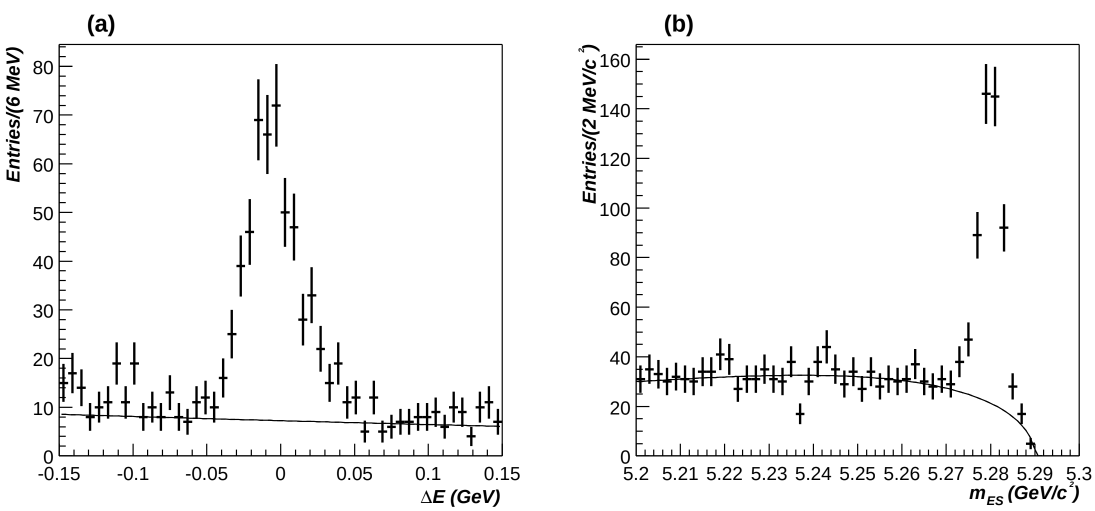

Figure 5: On-resonance signal region ΔE (a) and $m_{\rm ES}$ (b) distributions for $B^{\pm} \rightarrow K^{\pm}K^{\mp}K^{\pm}$. The solid lines show the expected level of continuum background, using appropriately normalised background shapes from the sideband regions in on-resonance data.

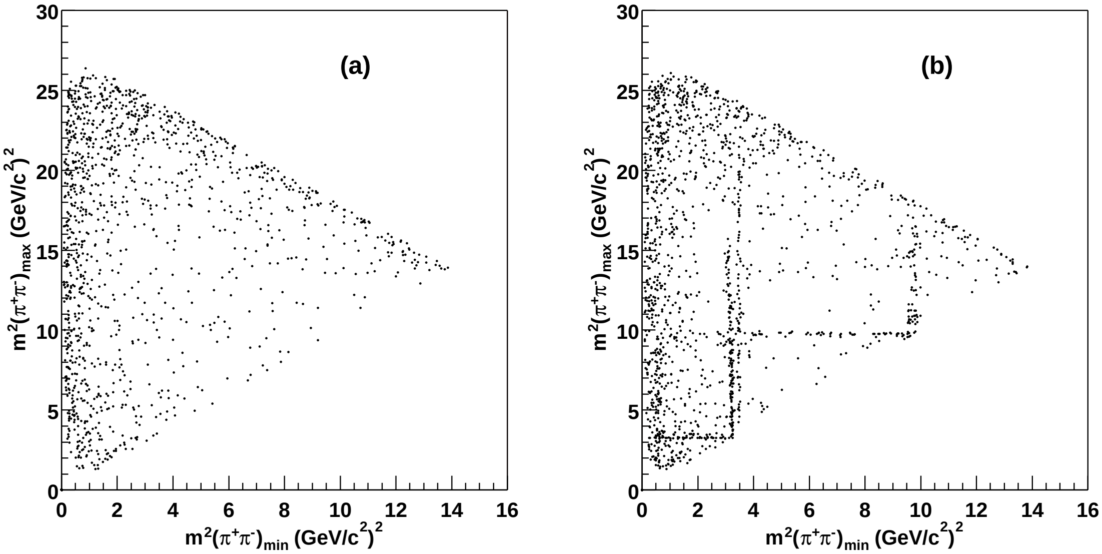

Figure 6: Unbinned Dalitz plots for on-resonance data for $B^{\pm} \to \pi^{\pm}\pi^{\mp}\pi^{\pm}$ for GSB region (a) and signal region (b). No efficiency corrections have been applied, and the open charm contributions are included in the plots.

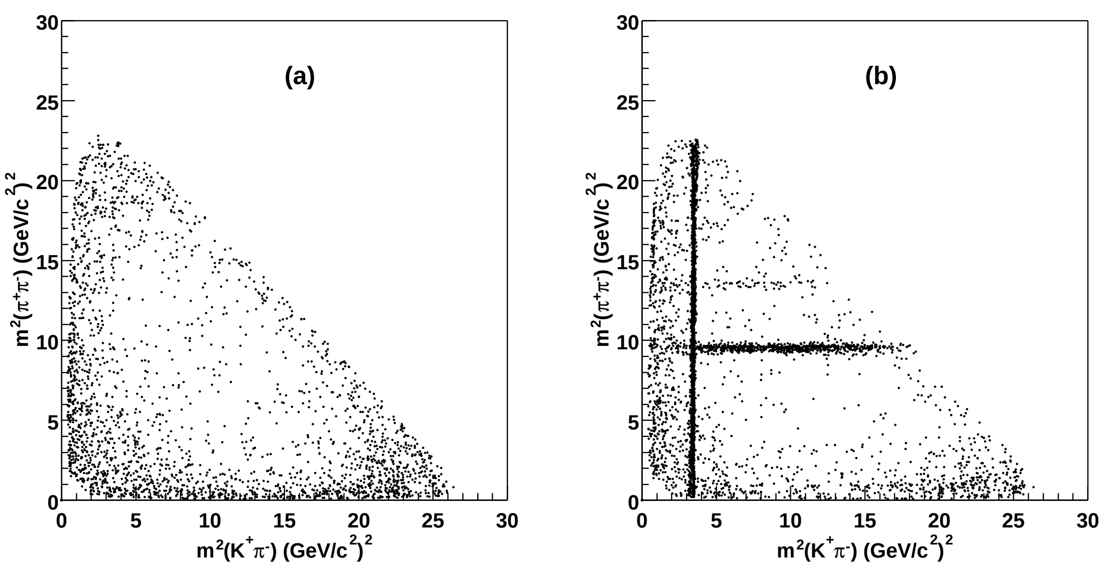

Figure 7: Unbinned Dalitz plots for on-resonance data for $B^{\pm} \to K^{\pm}\pi^{\mp}\pi^{\pm}$ for GSB region (a) and signal region (b). No efficiency corrections have been applied, and the open charm contributions are included in the plots.

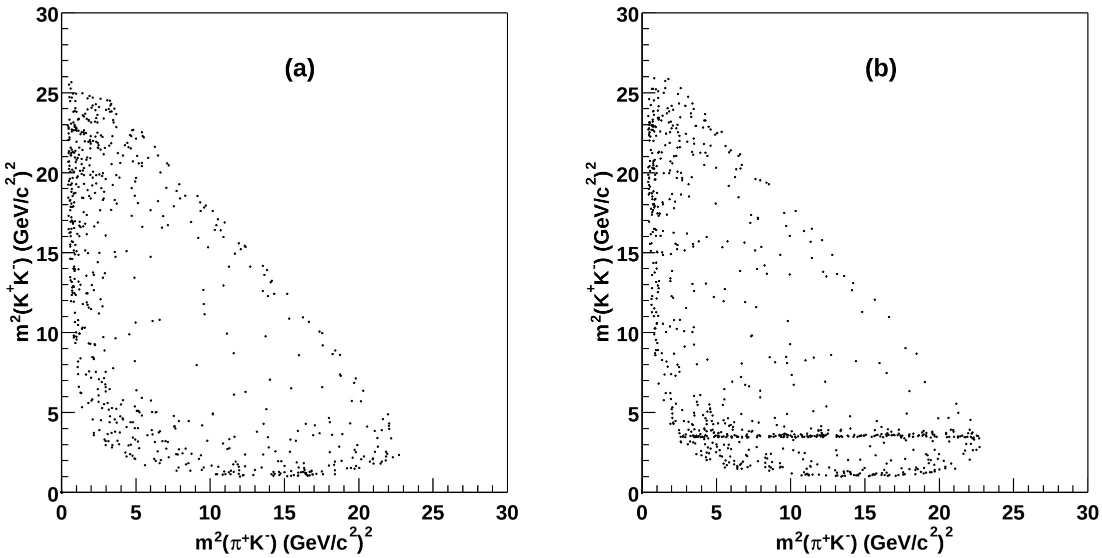

Figure 8: Unbinned Dalitz plots for on-resonance data for $B^{\pm} \to K^{\pm}K^{\mp}\pi^{\pm}$ for GSB region (a) and signal region (b). No efficiency corrections have been applied, and the open charm contributions are included in the plots.

6 Summary

We have obtained preliminary branching fractions for $B^{\pm} \to K^{\pm}\pi^{\mp}\pi^{\pm}$ and $B^{\pm} \to K^{\pm}K^{\mp}K^{\pm}$ over the whole Dalitz plot, and have determined conservative 90% upper limits for $B^{\pm} \to \pi^{\pm}\pi^{\mp}\pi^{\pm}$ and $B^{\pm} \to K^{\pm}K^{\mp}\pi^{\pm}$. The results are summarised in Table 5, where the results from BELLE [6] are also included for comparison.

Table 5: Branching fraction results from *BABAR* and BELLE.

Decay mode	*BABAR*	BELLE
$\pi^{\pm}\pi^{\mp}\pi^{\pm}$	$< 15 \times 10^{-6}$	—
$K^{\pm}\pi^{\mp}\pi^{\pm}$	$(59.2 \pm 4.7 \pm 4.9) \times 10^{-6}$	$(58.5 \pm 7.1 \pm 8.8) \times 10^{-6}$
$K^{\pm}K^{\mp}\pi^{\pm}$	$< 7 \times 10^{-6}$	$< 21 \times 10^{-6}$
$K^{\pm}K^{\mp}K^{\pm}$	$(34.7 \pm 2.0 \pm 1.8) \times 10^{-6}$	$(37.0 \pm 3.9 \pm 4.4) \times 10^{-6}$

7 Acknowledgments

We are grateful for the extraordinary contributions of our PEP-II colleagues in achieving the excellent luminosity and machine conditions that have made this work possible. The success of this

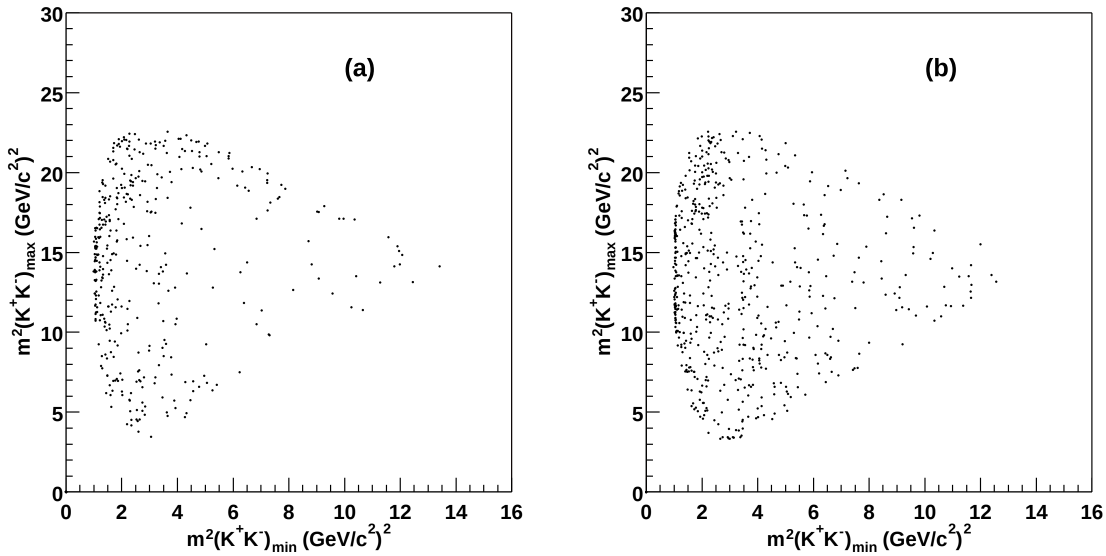

Figure 9: Unbinned Dalitz plots for on-resonance data for $B^\pm \to K^\pm K^\mp K^\pm$ for GSB region (a) and signal region (b). No efficiency corrections have been applied, and the open charm contributions are included in the plots.

project also relies critically on the expertise and dedication of the computing organizations that support *BABAR*. The collaborating institutions wish to thank SLAC for its support and the kind hospitality extended to them. This work is supported by the US Department of Energy and National Science Foundation, the Natural Sciences and Engineering Research Council (Canada), Institute of High Energy Physics (China), the Commissariat à l'Energie Atomique and Institut National de Physique Nucléaire et de Physique des Particules (France), the Bundesministerium für Bildung und Forschung (Germany), the Istituto Nazionale di Fisica Nucleare (Italy), the Research Council of Norway, the Ministry of Science and Technology of the Russian Federation, and the Particle Physics and Astronomy Research Council (United Kingdom). Individuals have received support from the A. P. Sloan Foundation, the Research Corporation, and the Alexander von Humboldt Foundation.

References

[1] R.E. Blanco, C. Gobel, and R. Mendez-Galain, "A New Method to Measure the CP Violating Phase γ Using $B^\pm \to \pi^\pm\pi^+\pi^-$ and $B^\pm \to K^\pm\pi^+\pi^-$ Decays", Phys. Rev. Lett. **86**, 2720 (2001), hep-ph/0007105.

[2] *BABAR* Collaboration, B. Aubert *et al.,* "The *BABAR* Detector", Nucl. Instr. and Meth. **A479**, 1 (2002), hep-ex/0105044.

[3] CLEO Collaboration, D. M. Asner *et al.,* "Search for Exclusive Charmless Hadronic B Decays", Phys. Rev. D **53**, 1039 (1996), hep-ex/9508004.

[4] ARGUS Collaboration, H. Albrecht *et al.,* "Exclusive Hadronic Decays of B Mesons", Z. Phys. C **48**, 543 (1990).

[5] Particle Data Group, D. E. Groom *et al.,* Eur. Phys. Jour. C **15**, 1 (2000).

[6] BELLE Collaboration, K. Abe *et al.,* "Study of Three Body Charmless B Decays", Phys. Rev. D **65**, 092005 (2002), hep-ex/0201007